J Fluoresc (2008) 18:131–137
DOI 10.1007/s10895-007-0251-8

ORIGINAL PAPER

Spectroscopic Properties of Er^{3+}/Yb^{3+}-codoped $PbO–Bi_2O_3–Ga_2O_3–GeO_2$ Glasses

G. F. Yang · D. M. Shi · Q. Y. Zhang · Z. H. Jiang

Received: 12 April 2007 / Accepted: 4 September 2007 / Published online: 2 October 2007

Abstract We investigate the spectroscopic properties of the 1.5-μm emission from the $^4I_{13/2} \rightarrow {}^4I_{15/2}$ transition of Er^{3+} ions in $PbO–Bi_2O_3–Ga_2O_3–GeO_2$ glasses for applications in broadband fiber amplifiers. The measured emission peak locates at 1,532 nm with a full width at half-maximum of ~45 nm. The glasses exhibit a large stimulated emission cross-section of 0.89×10^{-20} cm^2 and a large FWHM × σ_e^{peak} product of 40.0. Infrared-to-green upconversion occurs simultaneously upon excitation of the 1.5-μm emission with a commercially available 980 nm laser diode. The green-upconversion intensity has a quadratic dependence on incident pump laser power, indicating a two-photon process. Energy transfer processes and nonradiative phonon-assisted decays could account for the population of the $^2H_{11/2}$ of Er^{3+}. The results indicate the possibility towards the development of lead–bismuth–gallate–germanate based glasses as photonics devices.

Keywords Heavy-metal oxide glasses · Spectroscopic properties · Er^{3+} · Upconversion

Introduction

The optical properties of rare-earth (RE) doped glasses have been investigated extensively over the last several years. In particular, significant effort has been devoted to develop optimized glasses for broadband fiber amplifier, efficient lasing, and frequency upconversion due to their potential applications in various photonics devices [1, 2]. Erbium ion has been recognized as one of the most efficient RE ions for obtaining laser emission, frequency upconversion, and also in optical amplifiers and waveguide lasers, when doped in different hosts. Frequency upconversion in a variety of Er^{3+}-doped materials has been reported by many researchers [3, 4]. Er^{3+}-doped glass fiber amplifier and waveguide laser are very attractive for their use in 1.5-μm optical telecommunication networks and have been demonstrated in silicate, phosphate and fluoride glasses [1, 2, 5].

Amongst the variety of existing glasses, heavy-metal oxide (HMO) glasses are becoming more interesting and attractive for photonics in recent years, because of their high refractive index and low cutoff phonon energy compared with other oxide glasses such as silicate or phosphate glasses [6, 7]. In addition, a large amount of RE ions could be introduced in the HMO matrix. These HMO could be used in the production of optical fibers and planar waveguides [4]. The reduced phonon energy increases the quantum efficiency of luminescence from excited states of RE ions in these matrices and hence provides a possibility to develop more efficient lasers and fiber amplifiers at longer wavelengths compared to the other oxide glasses. These special optical properties make them important candidates for photonic devices. $PbO–Bi_2O_3–Ga_2O_3$ system has recently been investigated as a potential host for broadband fiber-optic amplifiers and all-solid-state upconversion lasers especially due to its advantages [6–10]. In this paper, we present the development and a detailed experimental investigation on the spectroscopic properties of Er^{3+}/Yb^{3+}-codoped $PbO–Bi_2O_3–Ga_2O_3–GeO_2$ (PBGG) glasses. The addition of GeO_2 in the batch could enhance the thermal stability of the glass against crystallization [10]. The Judd–

G. F. Yang · D. M. Shi · Q. Y. Zhang (✉) · Z. H. Jiang
Key Lab of Specially Function Materials of Ministry of Education, and Institute of Optical Communication Materials, South China University of Technology, Guangzhou 510641, People's Republic of China
e-mail: qyzhang@scut.edu.cn

G. F. Yang
e-mail: gfyang@scut.edu.cn

Ofelt (JO) parameters of Er^{3+} in the glasses and several important optical properties, such as the spontaneous emission probability, the fluorescence branching ratio, and the radiative lifetime, have been calculated by using the JO theory.

Experimental details

Lead–bismuth–gallate–germanium glasses of molar composition $(99.9-x)(36PbO–32Bi_2O_3–12Ga_2O_3–20GeO_2)–0.1Yb_2O_3–xEr_2O_3$ (x=0.05, 0.1, 0.2 and 0.5, named S1, S2, S3, and S4, respectively) were prepared by melting 15 g batches with the reagent-grade chemicals of PbO (99.8%), Bi_2O_3 (99.8%), Ga_2O_3 (99.98%), GeO_2 (99.8%), Er_2O_3 (99.99%), and Yb_2O_3 (99.99%) in a platinum crucible with a cover for 20 min at 1,050°C. The melts were then poured onto a stainless steel plate and annealed near the glass transition temperature for 1 h. After annealling, the samples for optical and spectral properties measurements were sliced into rectangular 15×15×1.5 mm^3 shape and optically polished.

The absorption spectra were obtained with the PERKIN-ELMER-LAMBDA 900 UV/VIS/NIR spectrophotometer from 400 to 1,700 nm with a resolution of 1 nm. The fluorescence spectra were measured on a computer-controlled TRIAX 320 spectrofluorimeter (Jobin-Yvon Inc.) upon excitation of a 980 nm laser diode (LD) as an excitation source. Emitted light was focused on to the monochromator and was monitored at the exit slit by a photon-counting R5108 photomultiplier tube (400–1,200 nm) for the visible up-conversion emission and *OREL SP71905* InGaAs detector (800–1,650 nm) for 1.5-μm emission. In order to compare the fluorescence intensity of Er^{3+} ions in different samples, the position and power (500 mW) of the pumping beam (focus radius of 0.4 mm on the test glasses) and the width (0.5 mm) of the slit used to collect the luminescence signal were fixed under the same conditions. The temporal decay curves of the fluorescence signals for 1,550 nm band of Er^{3+} were stored after averaging 128 times by a Tektronix TDS3012B digital phosphor oscilloscope. The lifetimes of $^4I_{13/2}$ levels were obtained from the first e-folding time of decay curves by using a computer-controlled digitizing oscilloscope through InGaAs detector (800–1,650 nm) excited at 980 nm excitation. All the optical measurements were performed at room temperature.

Results and discussion

Absorption spectra and JO analysis

Figure 1 shows the room temperature absorption spectra of Er^{3+}/Yb^{3+}-codoped lead–bismuth–gallate germanate glasses. The each band assignment, which corresponds to the upper level of transitions originating from the Er^{3+} ground multiplet ($^4I_{15/2}$), is also indicated in the figure. The absorption line shapes of all samples are similar with no shift in the absorption peaks. The intensities of the bands vary linearly with the concentration of Er^{3+} ions. Variations in the integral absorption intensities, Σ_{abs}, of the $^4I_{15/2} \rightarrow {}^4I_{13/2}$ transition as a function of Er^{3+} ions concentration, N_{Er}, are presented in inset of Fig. 1, showing a good linearity as the N_{Er} is from 1.75×10^{19} to 1.74×10^{20} ions/cm^3, which indicates that the studied glasses have good homogeneity and high solubility of Er_2O_3.

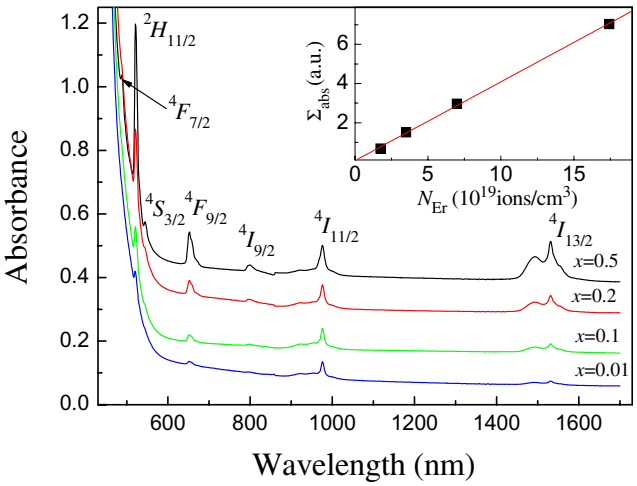

Fig. 1 Absorption spectra of Er^{3+}/Yb^{3+}-codoped PBGG glasses. The inset shows the variations in the integral absorption intensities, Σ_{abs}, of the $^4I_{15/2} \rightarrow {}^4I_{13/2}$ transition as a function of Er^{3+} ions concentration, N_{Er}. The line is obtained according to the linear regression (the linear regression equation is $\Sigma_{abs} = 0.068 + 0.402N_{Er}$) and the correlation coefficient is 0.999

The JO theory has often been used to calculate the spectroscopic parameters, such as strength parameters, spontaneous emission probability, branching ratio, and radiation lifetime, of REs in various matrixes. The three parameters Ω_t (t=2, 4, 6) can be obtained experimentally from the measured absorption spectrum and the refractive index of the host material employing the least-squares fitting by Eq. 1 [11, 12]:

$$S_{ed} = \sum_{t=2,4,6} \Omega_t \left| \left\langle [\alpha SL]J \left\| U^{(t)} \right\| [\alpha' S' L']J' \right\rangle \right|^2 \quad (1)$$

where S_{ed} is the line strength for electric dipole transitions between J manifolds; J and J' is the total angular momentum of the initial level and the terminal level, respectively; the matrix elements $U^{(t)}$ is given in reference [13]. Table 1 shows comparison of the JO intensity parameters, Ω_t (t=2, 4, 6), of Er^{3+} in various glass hosts. According to previous studies [14], Ω_2 is related with the symmetry of the glass hosts while Ω_6 is inversely proportional to the covalency of Er–O bond. The Er–O

Table 1 Judd–Ofelt intensity parameters of Er^{3+} in various glass hosts

Glasses	Ω_2 (10^{-20} cm^2)	Ω_4 (10^{-20} cm^2)	Ω_6 (10^{-20} cm^2)	Reference
S4	3.65	1.45	0.49	This work
Tellurite	4.12	1.81	0.85	14
Silicate	4.23	1.04	0.61	19
Phosphate	6.65	1.52	1.11	19
Aluminate	5.60	1.60	0.61	19
Germanate	5.81	0.85	0.28	19
Fluoride	2.91	1.27	1.11	19

bond is assumed to be dependent on the local basicity around the RE sites, which can be adjusted by the composition or structure of the glass hosts. It should be mentioned here that the Ω_6 value in PBGG is lower than that of fluoride, silicate, aluminate, and tellurite glass and larger than that of germante glass, which maybe due to introducing GeO_2 into the glass.

Table 2 represents the calculated results of the electric–dipole transition probabilities, A_{ed}, and magnetice–dipole transition probabilities, A_{md}, and radiative lifetimes, τ_{rad}, of sample S4. The total radiative rate, A_r, exhibits the large radiative transition probability (≈300 s^{-1}) for the $^4I_{13/2}$ level of Er^{3+}, which can be calculated by [15]:

$$A_r = A_{ed} + A_{md} = \frac{64\pi^4 e^2}{3h\lambda_m^3(2J+1)} \times \left[\frac{n(n^2+2)^2}{9} S_{ed} + n^3 S_{md}\right] \quad (2)$$

where h is the Planck constant, e is the elementary charge, n is the refractive index, λ is the mean wavelength of the absorption band. S_{md} is the line strength for magnetic dipole transitions between J manifolds when the transitions subject to the selection rules ΔS=ΔL=0, ΔJ=0, ±1 in Russel–Saunders limit:

$$S_{md} = \frac{1}{4m^2c^2} |\langle [\alpha SL]J \| L + 2S \| [\alpha' S' L'] \rangle J'|^2 \quad (3)$$

where the matrix elements $M = |\langle [S,L]J \| L + 2S \| [S', L'] J' \rangle|$ between SLJ states is for $J'=J-1$

$$M = \hbar \left\{ \left[(S+L+1)^2 - J^2 \right] \left[J^2 - (L-S)^2 \right] \Big/ 4J \right\}^{1/2} \quad (4)$$

for $J'=J$,

$$M = \hbar \left[(2J+1)/4J(J+1) \right]^{1/2} [S(S+1) - L(L+1) + 3J(J+1)] \quad (5)$$

for $J'=J+1$,

$$M = \hbar \left\{ \left[(S+L+1)^2 - (J+1)^2 \right] \left[(J+1)^2 - (L-S)^2 \right] \Big/ 4(J+1) \right\}^{1/2} \quad (6)$$

where $\hbar = h/2\pi$, J is the total angular momentum, L is the orbit angular momentum, and S is the total spin-orbin angular momentum. The A_r in the studied glass is much larger than that in silicate and phosphate glasses, due to the higher refractive index, indicates an enhanced local field and a larger radiative transition rate of Er^{3+} in the PBGG glasses.

The absorption cross-section of $^4I_{15/2} \rightarrow {}^4I_{13/2}$ transition was determined from the absorption spectra, and the stimulated emission cross-section of 1.53 μm band emission can be calculated by using McCumber theory [16]:

$$\sigma_e(\lambda) = \sigma_a(\lambda) \exp\left[(\varepsilon - h\upsilon)/kT\right] \quad (7)$$

where σ_2 and σ_e are absorption and stimulated emission cross-section, respectively, h is the Planck constant, k is the Boltzmann constant, υ is the photon frequency, ε is the net free energy required to excite one Er^{3+} from the $^4I_{15/2}$ state to $^4I_{13/2}$ at temperature T. The σ_2 and ε values can be calculated according to the experimentally obtained absorp-

Table 2 Energy gap ΔE, the spontaneous emission probability A, the fluorescence branching ratios β, and the radiative lifetime τ_{rad} of Er^{3+} ion at room temperature

Transition	Energy gap ΔE, (cm^{-1})	A (s^{-1})		Branching ratios, β, %	τ_{rad}(ms)
		A_{ed} (s^{-1})	A_{md} (s^{-1})		
$^4I_{13/2} \rightarrow {}^4I_{15/2}$	6,532	174.0	119.3	1	3.41
$^4I_{11/2} \rightarrow {}^4I_{15/2}$	10,246	238.1		78.3	3.29
$^4I_{13/2}$	3,714	29.1	37.0	21.7	
$^4I_{9/2} \rightarrow {}^4I_{15/2}$	12,516	383.2		84.3	
$^4I_{13/2}$	5,984	64.0		14.1	2.20
$^4I_{11/2}$	2,270	0	7.1	1.6	
$^4F_{9/2} \rightarrow {}^4I_{15/2}$	15,152	3,334.0		92.2	
$^4I_{13/2}$	8,620	179.4		5.0	0.28
$^4I_{11/2}$	4,906	94.6		2.6	
$^4I_{9/2}$	2,636	6.1		0.2	
$^4s_{3/2} \rightarrow {}^4I_{15/2}$	18,282	1,564.4		66.6	
$^4I_{13/2}$	11,750	632.7		26.9	0.43
$^4I_{11/2}$	8,036	52.2		2.2	
$^4I_{9/2}$	5,766	101.3		4.3	
$^4H_{11/2} \rightarrow {}^4I_{15/2}$	19,048	16,929.5			
$^4F_{7/2} \rightarrow {}^4I_{15/2}$	20,450	5,085.3			
$^4F_{5/2} \rightarrow {}^4I_{15/2}$	21,915	1,758.7			

tion spectra and the simplified procedure provided in Ref [17]. The absorption and stimulated emission cross-section of Er^{3+} in PBGG glass with x=0.5 are shown in Fig. 2. The stimulated emission cross-section is proportional to the refractive index of the glass host [$\sigma_e \sim (n^2+2)^2/n$] [18]. Since the PBGG glasses have a large refractive index (~2.26), it is expected that Er^{3+} in PBGG glass is capable of providing large stimulated emission cross-section (the peak of stimulated emission cross-section is 0.89×10^{-20} cm^2) at the 1.53 μm bands, which is much higher than those of the silicate [19], phosphate [20] and ZBLAN [21] glasses.

Fluorescence spectra and lifetime

Figure 3a illustrates the emission spectrum of Er^{3+} in sample S4. The measured peak wavelength and full width at half maximum (FWHM) of the fluorescent, which is defined as the wavelength difference between the two x values at the half-maximum of the peak of the measured fluorescent, are 1,530 and 45 nm, respectively. The Er^{3+} emission spectra in PBGG glasses are significantly broader compared with the silicate, phosphate, and germanate glass as potential Er^{3+}-doped fiber amplifier (EDFA) hosts. The inset in Fig. 3b shows decay lifetime of the Er^{3+}:$^4I_{13/2}$ level excited by 980 nm LD. It is seen that the emission decay kinetics could be expressed by simply exponential. The dependence of the lifetime upon the Er^{3+} concentration is shown in Fig. 3b. It has been clearly seen that the lifetimes increased from 3.1 to 4.2 ms with an increase of Er^{3+} concentration, which maybe due to the radiation trapping [22].

The gain bandwidth of an amplifier is determined largely by the FWHM of the emission spectrum and the stimulated emission cross-section. A figure-of merit (FOM) for bandwidth as the product FWHM×σ_e [19, 23] is listed in Table 3. The FWHM×σ_e product is critical quality parameters for EDFA. Larger values of the FWHM×σ_e product implies wider gain bandwidth. The calculated values of the FWHM×σ_e product of the PBGG glasses are in the range of 388–401. It should be mentioned here that the values of FWHM×σ_e of the PBGG glasses are much higher than that of the silicate, phosphate and ZBLAN glasses and are comparable with the tellurite glass as a host material for Er^{3+} doped for a broadband amplifier.

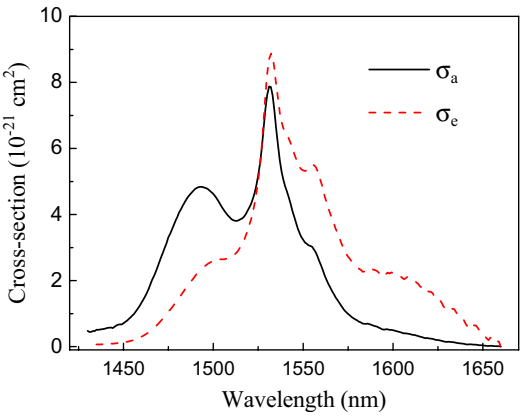

Fig. 2 Cross section of the absorption for the $^4I_{15/2} \rightarrow {}^4I_{13/2}$ transition and the emission fot the $^4I_{13/2} \rightarrow {}^4I_{15/2}$ transition in PBGG glass (x=0.5)

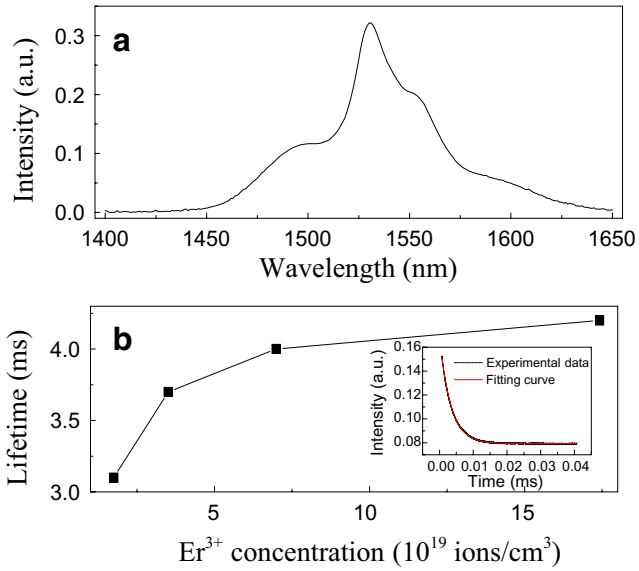

Fig. 3 The emission spectrum of Er^{3+} in sample S4 (**a**) and the dependence of the lifetime upon the Er^{3+} concentration (**b**). The *inset* shows decay lifetime of the Er^{3+}:$^4I_{13/2}$ level excited by 980 nm LD

Upconversion emission properties of Er^{3+} ions in PBGG glass

When the glass is excited upon 980 nm LD, an intense green-upconversion has been noticed by the naked eye. The recorded room temperature upconversion fluorescence spectra of samples upon excitation of a 500 mW 980 nm LD are shown in Fig. 4. The upconversion fluorescence at approximately 525, 547 and 660 nm, are assigned to the $^2H_{11/2} \rightarrow {}^4I_{15/2}$, $^2S_{3/2} \rightarrow {}^4I_{15/2}$, and $^4F_{9/2} \rightarrow {}^4I_{15/2}$ transitions of Er^{3+} ions, respectively. The result indicates that lasing could be expected from either the green or the red transitions with a suitable choice of cavity mirrors.

Table 3 Comparisons of σ_e, FWHM and FWHM×σ_e of Er^{3+} in different glass hosts

Glasses	σ_e ($\times10^{-21}$ cm^2)	FWHM (nm)	FWHM×σ_e	Reference
PBGG	8.91–10.21	38–45	388–401	This work
Silicate	5.5	40	220	19
Tellurite	7.5	65	488	19
Phosphate	6.4	37	237	20
ZBLAN	5.7	42	302	21

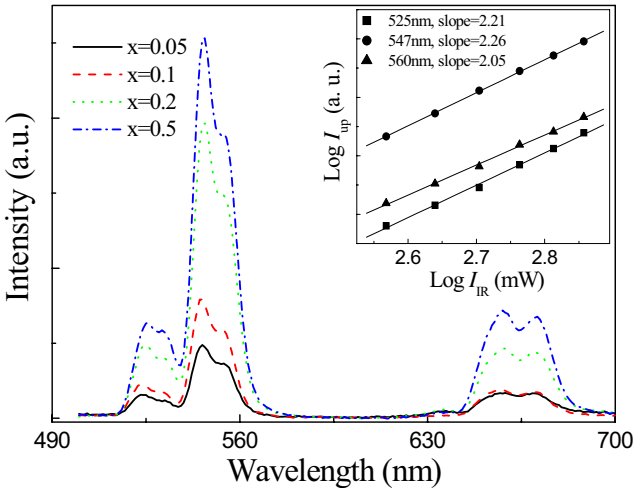

Fig. 4 Upconversion luminescence spectra of PBGG glasses. The *inset* shows the dependence of upconversion fluorescence intensity on excitation power under 980 nm excitation in the glasses

In an upconversion process, the upconversion emission intensity I_{up} is proportional to I_{IR}^{n}, where I_{IR} and n represent the intensity of the excitation light and the number of photons absorbed per up-converted photon emitted [24, 25], respectively. A plot of logI_{up} vs logI_{IR} yields a straight line with slope n. The inset of Fig. 4 shows such plots for the 525, 547, and 660 nm emission in PBGG glass (x=0.5) under 980 nm excitation. The obtained ns, 2.21, 2.26, and 2.05, are corresponding to the 525, 547, and 660 nm emission, respectively, indicating two-photon processes. Based on above disscussed results, upconversion excitation mechanisms has been proposed to be involved in the population of the relevant excited-state emitting levels of the Er^{3+}/Yb^{3+}-codoped glass as following, shown in Fig. 5: (1) Er^{3+} ion is firstly excited from the ground state $^4I_{15/2}$ to the excited state $^4I_{11/2}$ through one of the following three processes under 980 nm excitation: (I) ground-state absorption (GSA): $^4I_{15/2}$ (Er^{3+}) + a photon → $^4I_{11/2}$ (Er^{3+}),

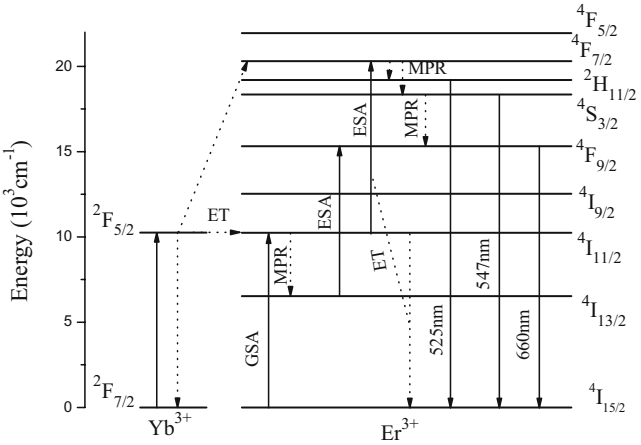

Fig. 5 Schematic energy level diagram and upconversion process of Er^{3+}/Yb^{3+}–codoped PBGG glasses

(II) phonon-assisted energy transfer (PAET) from the Yb^{3+} $^2F_{5/2}$ state:$^2F_{5/2}$ (Yb^{3+}) + $^4I_{15/2}$ (Er^{3+}) → $^2F_{7/2}$ (Yb^{3+}) +$^4I_{11/2}$ (Er^{3+}), and (III) energy transfer (ET) from the $^4I_{11/2}$ state of adjacent Er^{3+}. Among the aforementioned three processes, PAET from Yb^{3+} is the dominant one, due to the larger absorption cross section of Yb^{3+} at around 980 nm. (2) The ions at the populated $^4I_{11/2}$ state are promoted to the $^4F_{7/2}$ state by one of the following three processes: (I) excited-state absorption (ESA): $^4I_{11/2}$ (Er^{3+}) + a photon → $^4F_{7/2}$ (Er^{3+}), (II) PAET from Yb^{3+}:$^2F_{5/2}$ (Yb^{3+}) + $^4I_{11/2}$ (Er^{3+}) → $^2F_{7/2}$ (Yb^{3+}) + $^4F_{7/2}$ (Er^{3+}), and (III) ET from the $^4I_{11/2}$ state of adjacent Er^{3+}: $^4I_{11/2}$ + $^4I_{11/2}$ → $^4F_{7/2}$ + $^4I_{15/2}$. Er^{3+} ions at the populated $^4F_{7/2}$ state can relax nonradiative relaxation (NR) very fast to the intermediate state of $^2H_{11/2}$ due to a multiphonon relaxation process (MPR), the $^2H_{11/2}$ → $^4I_{15/2}$ transition shows the 525 nm green emission. Er^{3+} ion at the $^4F_{7/2}$ state can also decay rapidly down to the $^4S_{3/2}$ state, and finally, the $^4S_{3/2}$→$^4I_{15/2}$ transition reveals an intense green-upconversion at 547 nm. For the red-upconversion emission at 660 nm, Er^{3+} ion is first excited from the ground state $^4I_{15/2}$ to the excited $^4I_{11/2}$ through the aforementioned three processes: GSA, PAET and ET under 980 nm excitation. The Er^{3+} ions populated $^4I_{11/2}$ state then decays NR to the long-living $^4I_{13/2}$ state due to MRP, and are promoted to the $^4F_{9/2}$ state by one of the following processes: (I) ESA: $^4I_{13/2}$ (Er^{3+}) + a photon → $^4F_{9/2}$ (Er^{3+}), (II) PAET from Yb^{3+}: $^2F_{5/2}$(Yb^{3+}) + $^4I_{13/2}$ (Er^{3+}) → $^2F_{7/2}$ (Yb^{3+}) + $^4F_{9/2}$ (Er^{3+}), and (III) ET from the $^4I_{11/2}$ state of adjacent Er^{3+}: $^4I_{11/2}$ + $^4I_{13/2}$ →$^4I_{15/2}$ + $^4F_{9/2}$, and also (IV) a contribution from higher-energy state $^4S_{3/2}$ through a NR, and finally, the $^4F_{9/2}$ → $^4I_{15/2}$ transition gives 660 nm red emission.

The ESA and ET are the dominant processes in the involved upconversion mechanisms of Er^{3+} ions. ESA is a single ion process and independent of the ion concentration in the glass. The intensities of green emission does not change between the PBGG glasses with x=0.05 and x=0.1, which indicates that the dominant mechanism for the $^4F_{9/2}$ → $^4I_{15/2}$ transition is ESA and the ET rarely occurs between excited ions when the Er^{3+} concentration is low. The ET process depends on the Er^{3+} ion concentration in the glass. A remarkable increase of upconversion emission intensity with an increase of the Er^{3+} concentration from 0.1 up to 0.5 mol% has been observed, which results from ET between the excited Er^{3+} ions when the

Table 4 The values of I_{525nm}/I_{547nm} and I_{660nm}/I_{547nm} with various Er^{3+} concentrations

Er^{3+} concentration, mol%	I_{525nm}/I_{547nm}	I_{660nm}/I_{547nm}
0.05	0.293	0.313
0.1	0.271	0.212
0.2	0.247	0.229
0.5	0.243	0.269

distance between the two excited Er^{3+} ions is short. On the other hand, when Er^{3+} concentration increases ($x \geq 0.1$), the intensity of red emission, $I_{660\ nm}$, increases much faster than that of green emission, $I_{547\ nm}$, for the value of $I_{660\ nm}/I_{547\ nm}$ (see Table 4) increases with Er^{3+} concentration increasing. It is indicated that the dominant population of the $^4F_{9/2}$ state is the total result of ESA and ET from $^4I_{13/2}$ state. The Er^{3+} ions at the $^2H_{11/2}$ state can decay to the $^4S_{3/2}$ state due to the multiphonon relaxation process. The estimated energy gap between the $^2H_{11/2}$ state and the next lower state $^4S_{3/2}$ state is ~800 cm^{-1}, but it is about 3,200 cm^{-1} between the $^4S_{3/2}$ state and the next lower $^4F_{9/2}$ state. Thus, multiphonon relaxation rate is much larger from $^2H_{11/2} \rightarrow {}^4S_{3/2}$ than that of $^4S_{3/2} \rightarrow {}^4F_{9/2}$, which resulting the 525 nm emission intensity decrease. It leads to the value of $I_{525\ nm}/I_{547\ nm}$ decreases with the Er^{3+} concentration increasing, as listed in Table 4.

Based on above results, we would like to suggest PBGG glasses codoped with Er^{3+}/Yb^{3+} as more promising and useful optical materials towards the development of optical amplifier and up-conversion laser glass materials, respectively. However, an important point should be noted that the upconversion emissions must be controlled when the glass is used in broadband 1.5-μm optical amplifier.

Conclusion

In summary, we report on the spectroscopic properties of a new glass system PbO–Bi_2O_3–Ga_2O_3–GeO codoped with Er^{3+}/Yb^{3+}. A broadband 1.5-μm emission with a measured peak wavelength of 1,532 nm and FWHM of ~45 nm has been observed upon excitation with a conventional 980 nm LD. An intense room temperature green-upconversion has also been observed. From the optical absorption spectral measurements, the JO intensity parameters have been computed and the low values of Ω_2 and Ω_6 comparing to the values in conventional oxide glasses were found. The PBGG glass studied exhibits a large stimulated emission cross-section of 0.89×10^{-20} cm^2 and a large $FWHM \times \sigma_e^{peak}$ product of 401, which is larger than that of the conventional oxide glasses. The strong green-upconversion and large $FWHM \times \sigma_e^{peak}$ product of these PBGG glasses have demonstrated a strong and promising potentiality towards the development of an oxide-based fiber amplifier and green-upconversion glass-fiber laser.

Acknowledgements The authors would like to thank Mr. Z M Feng for his technical assistance. This work is jointly supported by NSFC (50602017, 50472053), GSTG (Guangzhou, 2006J1-C0491), and NFSG (Guangdong, 05300221).

References

1. Digonnet MJF (2001) Rare-earth-doped fiber lasers and amplifiers. Marcel Dekker, New York
2. Reisfeld R, Jorgensen CK (1977) Lasers and excitated states of rare-earth. Springer, Berlin Heidelberg New York
3. Li T, Zhang QY, Liu YH, Zhang JJ, Deng ZD, Jiang ZH (2004) Infrared-to-visible upconversion and 1.53-μm emission of Er^{3+}-doped $Al(PO_3)_3$-based fluorophosphate glass. Chin Phys Lett 21:1147–1149
4. Oliveira AS, de Araujo MT, Gouveia-Neto AS, Sombra ASB, Neto JAM, Aranha N (1998) Upconversion fluorescence spectroscopy of Er^{3+}/Yb^{3+}-doped heavy metal Bi_2O_3–Na_2O–Nb_2O_5–GeO_2 glass. J Appl Phys 83:604–606
5. Jiang SB, Luo T, Hwang BS, Smekatala F, Seneschal K, Lucas J, Peyghambarian N (2000) Er^{3+}-doped phosphate glasses for fiber amplifiers with high gain per unit length. J Non-Cryst Solids 263:364–368
6. MacFarlane DR, Newman PJ, Plathe R, Booth DJ (1999) Heavy metal oxide glasses as active materials. Proc SPIE 3849: 94–102
7. Kharlamov AA, Almeida RM, Heo J (1996) Vibrational spectra and structure of heavy metal oxide glasses. J Non-Cryst Solids 202:233–240
8. Zhang QY, Li T, Jiang ZH (2005) 980 nm laser-diode-excited intense blue upconversion in Tm^{3+}/Yb^{3+}-codoped gallate–bismuth–lead glasses. Appl Phys Lett 87:171911
9. Kassab LRP, Tatumi SH, Mendes CMS, Courrol LC, Wetter NU (2000) Optical properties of Nd doped Bi_2O_3–PbO–Ga_2O_3 glasses. Opt Express 6:104–108
10. Song JH, Heo J, Park SH (2003) Emission properties of PbO–Bi_2O_3–Ga_2O_3–GeO_2 glasses doped with Tm^{3+} and Ho^{3+}. J Appl Phys 93:9441–9445
11. Judd BR (1962) Optical absorption intensities of rare-earth ions. Phys Rev B 127:750–761
12. Ofelt GS (1962) Intensities of crystal spectra and decay of Er^{3+} fluorescence in LaF_3. J Chem Phys 37:511–520
13. Weber MJ (1967) Probabilities for radiative and nonradiative decay of Er^{3+} in LaF_3. Phys Rev 157:262–272
14. Ohishi Y, Mori A, Yamada M, Ono H, Nishida Y, Oikawa K (1998) Gain characteristics of tellurite-based erbium-doped fiber amplifiers for 1.5-μm broadband amplification. Opt Lett 23: 274–276
15. Jacobs RR, Weber MJ (1976) Dependence of the $^4F_{3/2} \rightarrow {}^4I_{11/2}$ induced-emission cross section for Nd^{3+} on glass composition. IEEE J Quantum Electron 12:102–111
16. McCumber DE (1964) Theory of phonon-terminated optical masers. Phys Rev 134(2A):299–306
17. Miniscalco WJ, Quimby RS (1991) General procedure for the analysis of Er^{3+} cross sections. Opt Lett 16:258–260
18. Wang JS, Vogel EM, Snitzer E (1994) Tellurite glass: a new candidate for optical devices. Opt Mater 3:187–203
19. Zou XL, Izumitani T (1993) Spectroscopic properties and mechanisms of excited state absorption and energy transfer upconversion for Er3+-doped glasses. J Non-Cryst Solids 162:68–80
20. Jiang SB, Luo T, Hwang BS, Smekatala F, Seneschal K, Lucas J, Peyghambarian N (2000) Er^{3+}-doped phosphate glasses for fiber amplifiers with high gain per unit length. J Non-Cryst Solids 263:364–368
21. Shen SX, Naftaly M, Jha A (1999) Tm^{3+}- and Er^{3+}-doped tellurite glass fibers for a broadband amplifier at 1430 to 1600 nm. Proc SPIE 3849:103–110

22. Dai SX, Yang JH, Wen L, Hu LL, Jiang ZH (2003) Effect of radiative trapping on measurement of the spectroscopic properties of Yb^{3+}: phosphate glasses. J Lumin 104:55–63
23. Chen DD, Liu YH, Zhang QY, Deng ZD, Jiang ZH (2005) Thermal stability and spectroscopic properties of Er^{3+}-doped niobium tellurite glasses for broadband amplifiers. Mater Chem Phys 90:78–82
24. Pollnau M, Gamelin DR, Luthi SR, Gudel HU, Hehlen MP (2000) Power dependence of upconversion luminescence in lanthanide and transition-metal-ion systems. Phys Rev B 61:3337–3346
25. Muller P, Wermuth M, Gudel HU (1998) Mechanisms of near-infrared to visible upconversion in $CsCdBr_3$: Ho^{3+}. Chem Phys Lett 290:105–111